JGR Atmospheres

RESEARCH ARTICLE
10.1029/2021JD036206

Influence of the North Pacific Victoria Mode on the Spring Persistence Barrier of ENSO

Liang Shi[1], Ruiqiang Ding[2], Shujuan Hu[1], Jianping Li[3], Yuheng Tseng[4], and Xumin Li[5]

[1]Key Laboratory for SemiArid Climate Change of the Ministry of Education, College of Atmospheric Sciences, Lanzhou University, Lanzhou, China, [2]State Key Laboratory of Earth Surface Processes and Resource Ecology, Beijing Normal University, Beijing, China, [3]Laboratory for Regional Oceanography and Numerical Modeling, Qingdao National Laboratory for Marine Science and Technology, Qingdao, China, [4]Institute of Oceanography, National Taiwan University, Taipei, Taiwan, [5]Key Laboratory of Meteorological Disaster of Ministry of Education (KLME), Nanjing University of Information Science and Technology, Nanjing, China

Key Points:

- VM events have a robust impact on the persistence of ENSO SSTAs
- Strong VM events can extend the duration of ENSO SSTAs and decrease the intensity of the ENSO SPB
- Strong VM events are closely linked with two-winter ENSO events

Correspondence to:

R. Ding,
drq@mail.iap.ac.cn

Citation:

Shi, L., Ding, R., Hu, S., Li, J., Tseng, Y., & Li, X. (2022). Influence of the North Pacific Victoria mode on the spring persistence barrier of ENSO. *Journal of Geophysical Research: Atmospheres*, *127*, e2021JD036206. https://doi.org/10.1029/2021JD036206

Received 14 NOV 2021
Accepted 13 APR 2022

Author Contributions:

Conceptualization: Ruiqiang Ding
Data curation: Liang Shi
Project Administration: Ruiqiang Ding, Shujuan Hu
Supervision: Ruiqiang Ding, Shujuan Hu
Visualization: Liang Shi
Writing – original draft: Liang Shi
Writing – review & editing: Liang Shi, Ruiqiang Ding, Shujuan Hu, Jianping Li, Yuheng Tseng, Xumin Li

Abstract This study focuses on the influence of the North Pacific Victoria mode (VM) on the persistence of the sea surface temperature anomalies (SSTAs) of El Niño–Southern Oscillation (ENSO). Both observational data and outputs from phases 5 and 6 of the Coupled Model Intercomparison Project show that VM events can enhance the persistence of ENSO SSTAs and reduce the intensity of the spring persistence barrier (SPB) of ENSO SSTAs. The possible reasons for these phenomena are that the SSTAs develop (decay) slowly and do not experience a rapid sign reversal during their decaying phase, indicating a relatively weak ENSO SPB occurs in the spring for strong VM cases. However, during weak VM cases, they transit quickly from positive (negative) SSTAs into negative (positive) SSTAs. The amplitudes of the SSTAs during weak VM cases are relatively greater in the mature phase than those during strong VM cases, resulting in a relatively strong ENSO SPB. Furthermore, VM events can affect the strength of the westerly wind anomalies over the western Pacific. The magnitude of the westerly wind anomalies is weaker when a strong ENSO co-occurs with a strong VM event than when it is associated with a weak VM event. In addition, the subsurface water during the strong VM case transits slowly from positive to negative while that transits relatively fast during weak VM cases, which are consistent with the evolutions of SSTAs. Thus, they together affect the recharge/discharge oscillation process of ENSO, which eventually lead to a strong or a weak ENSO SPB phenomenon occurring in the spring during strong or weak VM cases, respectively. The findings offer a new sight for studying the persistence of ENSO SSTAs.

1. Introduction

El Niño–Southern Oscillation (ENSO) dominates the variability in the tropical Pacific at seasonal to interannual time scales and has a profound impact on the year-to-year variability of Earth's climate (Foltz & Mcphaden, 2006; Philander, 1990; Timmermann et al., 2018). It also has global impacts on human life and economic growth (e.g., agriculture, public health, droughts and floods, terrestrial ecosystems, and the global carbon cycle; Dai et al., 1998; Thirumalai et al., 2017). Hence, accurate prediction of ENSO is of considerable public interest. Fortunately, ENSO is one of the most predictable climate fluctuations on Earth, and, using both dynamical and statistical models, considerable efforts have been devoted to predicting ENSO at seasonal lead times. Both dynamical and statistical models have made remarkable achievements over the past 30 years, and reasonable predictions can now be made at up to two–three seasons in advance (An & Wang, 2005; Barnston et al., 2017; Tseng et al., 2016; Zheng et al., 2009).

However, the prediction skills of many models suffer from an abrupt and obvious decline across the boreal spring months (February–March–April; FMA)—a phenomenon referred to as the "spring persistence barrier" (SPB) of ENSO forecasts (Jin et al., 2008; Luo et al., 2008; McPhaden, 2003; Webster & Yang, 1992). It is a well-known characteristic of ENSO forecasts, but its causes are yet to be fully explained. Previous studies have proposed that the SPB is caused by the relatively weak ocean–air coupling over the Pacific during spring (Blumenthal, 1991; Torrence & Webster, 1998; Zebiak & Cane, 1987). Some studies have reported that the biennial component of ENSO and the phase-locking of ENSO to the annual cycle may also play a crucial role in causing the SPB (Clarke & Van Gorder, 1999; Yu, 2005). In addition, initial errors with certain specific patterns (Duan et al., 2009; Mu et al., 2007), the seasonality of connections to the subsurface ocean (Matei et al., 2008; Zhu et al., 2016), and

westerly wind burst activity (Chen et al., 2015; Lopez & Kirtman, 2014) can also affect the SPB of ENSO. Moreover, Hu et al. (2019) also indicate that SPB is essential a signal noise ratio (SNR) problem, while the anomaly signal is weak and the SNR is small in spring, thus, SPB is an inherent challenge to ENSO prediction.

Considering the important effects of the SPB on the prediction skill of ENSO, extensive studies have been conducted on different aspects of the SPB in an effort to determine how to reduce it. For example, several studies have pointed out that the SPB can be dramatically reduced after the signals from both the ocean and atmosphere (e.g., the oceanic heat content over the equatorial Pacific and the zonal wind stress along the tropical western Pacific) are considered properly during boreal spring (Chen et al., 2015; Lopez & Kirtman, 2014; Matei et al., 2008; McPhaden, 2003; Zhu et al., 2016). Masuda et al. (2015) indicated that the ENSO forecast skill across boreal spring can be greatly improved if long-term variations of the annual surface energy exchange (e.g., heat and momentum exchange through the sea surface) are considered in prediction models, as these factors characterize the evolution of El Niño. In addition, multi-model ensembles have been proven to be an effective approach to reducing the SPB (Wittenberg et al., 2014; Zheng et al., 2016).

Recently, many researches pointed out that the variations in the subtropical North Pacific are important for ENSO diversity, especially for CP El Niño based on the observation (Wang, Tan, & Wang, 2018; Yeh et al., 2015; Yu et al., 2010, 2012; Yu & Kao, 2007; Yu & Kim, 2011) and model results (Chen et al., 2021; Wang, Chen, et al., 2018; Wang, Guan, et al., 2018; Yu & Fang, 2018). Some other work further indicated that tropical Pacific (ENSO) can affect the North Pacific through generating a Pacific–North American like variation (Hu et al., 2014; Li et al., 2019; Wallace & Gutzler, 1981). Furthermore, a few studies have shown that both the extratropical North and South Pacific Oceans can also affect the occurrence and development of ENSO (Ashok et al., 2007; Ballester et al., 2011; Ding et al., 2016; Ham et al., 2013; Jin & Kirtman, 2009; Terray, 2010). In particular, some studies suggested that the Victoria mode (VM; Bond et al., 2003; Ding et al., 2015)—a decayed response of the SST footprint forced by the North Pacific Oscillation (NPO; Walker & Bliss, 1932)—can act as an oceanic bridge allowing wintertime extratropical atmospheric variability to influence subsequent ENSO events, either through the seasonal footprinting mechanism (SFM; Vimont, Battisti, & Hirst, 2003; Vimont, Wallace, & Battisti, 2003) or the trade wind charging (TWC) mechanism (Anderson, 2003; Anderson et al., 2013). Because VM reaches its peak around late winter and early spring and can serve as a precursor for subsequent ENSO events (Ding et al., 2015), it has been speculated that VM events may exert an influence on the SPB of ENSO. Thus, this paper investigates the impact of the VM on ENSO's SPB.

The remainder of the paper is arranged as follows: In Section 2, the data and methods used for analysis are presented. The influence of the VM on the SPB of ENSO in observational data is presented in Section 3. Section 4 investigates possible mechanism for why the VM can affect the persistence of ENSO SSTAs. Section 5 presents further analyses of the relationship between ENSO's SPB and VM by using the outputs from the phases 5 and 6 of the Coupled Model Intercomparison Project. And finally, Section 6 summarizes the major results of this paper.

2. Data Sets and Methods

2.1. Observational and Reanalysis Datasets

This paper utilizes the SST data from HadISST (the Hadley Centre Sea Ice and SST dataset) on a $1° \times 1°$ longitude–latitude grid for the period 1948–2020 (Rayner, 2003). For the analyses of atmospheric fields, the NCEP–NCAR (National Centers for Environmental Prediction–National Center for Atmospheric Research) reanalysis product on a $2.5° \times 2.5°$ horizontal grid is also used (Kalnay et al., 1996). The subsurface ocean temperature data (1948–2020) are from the ocean gridded products of the Institute of Atmospheric Physics, Chinese Academy of Sciences (Cheng et al., 2017). The monthly mean anomalies of all atmospheric and oceanic variables were computed with respect to the climatological monthly mean (1981–2010). To reduce the anthropogenic influence, the data and indices used in this study were linearly detrended before calculation.

In addition to the observational data, this paper also employs the outputs from the preindustrial simulations of 32 climate models that participated in CMIP5 and 6 (phases 5 and 6 of the Coupled Model Intercomparison Project; Eyring et al., 2016; Taylor et al., 2012). Given that the simulation length varies from model to model, outputs from the last 100 years of each run were used for the analysis.

Table 1
Co-Occurrence of Positive or Negative VM and ENSO Events During the Period 1950–2020

VM/ENSO		El Niño	La Niña
Strong	Positive	1957, 1963, 1965, 1968, 1986, 1991, 1997, 2014, 2015, 2018, 2019	
	Negative	2002	1988, 1998, 1999, 2000, 2001, 2007, 2008, 2010
Weak	Positive	1956, 1951, 1969, 1972, 1982, 1994, 2020	1950, 1955, 1964, 1971, 1974, 1984, 1995, 2005, 2016
	Negative	1953, 1976, 1977, 1987, 1979, 2004, 2006, 2009	1954, 1970, 1973, 1975, 1983, 2011, 2017

2.2. Index Definitions

The area-averaged SST over the Niño3.4 region (5°S–5°N, 170°–120°W) is used as the ENSO index in this paper (Trenberth, 1997). To examine the influence of the VM events on the persistence of ENSO SSTAs, we divide ENSO events into two cases according to the intensity of the Niño3.4 index at its peak phase: December(0) to February(1), where the numerals "0" and "1" indicate the developing and decaying year of ENSO, respectively. The Niño3.4 index at its peak time during the period 1950–2020, which has an intensity ≥1.0 or ≤1.0 (−1.0 < Niño3.4 index < −0.5 or 0.5 < Niño3.4 index < 1.0) standard deviation (SD), means a strong (weak) ENSO event (Table 1).

Following Bond et al. (2003) and Ding et al. (2015), we apply the empirical orthogonal function (EOF) analysis method to the monthly SSTAs over the North Pacific (20.5°–65.5°N, 124.5°E−100.5°W) for 1948–2020. The EOF1 mode is known as the Pacific Decadal Oscillation (PDO; Figure 1a; Walker & Bliss, 1932). The EOF2 mode, which is the VM, exhibits a northeast–southwest dipole SST spatial pattern with a band of positive SSTAs extending from the west coast of North America to the western Bering Sea and a band of negative SSTAs over the central and western North Pacific (Figure 1b). The principal component (PC) time series are defined as the PDO index (PDOI; PC1; Figure 1c) and the VM index (VMI; PC2; Figure 1d) after being standardized, respectively.

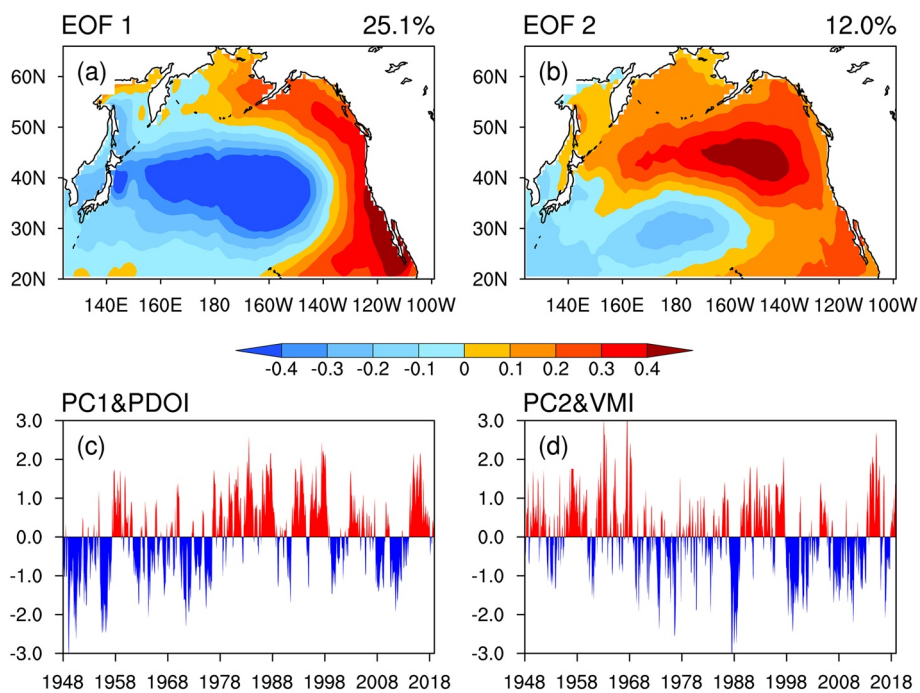

Figure 1. Spatial pattern of (a) EOF1 and (b) EOF2 of the North Pacific (20.5°—65.5°N, 124.5°E−100.5°W; after removing the global mean SST anomaly) monthly SSTA for the period 1948-2020. (c) and (d) are the corresponding PC1 (PDO) and PC2 (VMI) time series, respectively. EOF1 (EOF2) accounts for 25.1% (12.0%) of the total variance. EOF1 (EOF2) represents PDO mode (Victoria mode; VM).

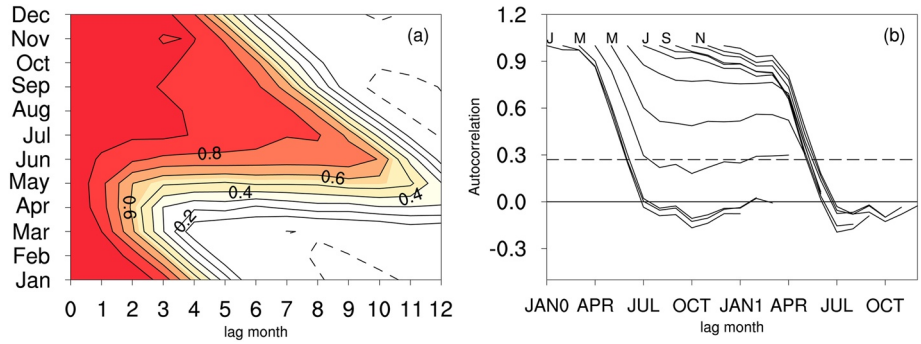

Figure 2. (a) Lagged autocorrelations (shading at the 95% significance level; ≥0.27) of the area-averaged SSTAs over the Niño3.4 region (5°S–5°N, 170°–120°W; Niño3.4 index) for the period 1950–2020. The contour interval is 0.1. (b) Autocorrelation curves of the Niño3.4 index for each of the 12 starting months shown in (a) as a function of time. For clarity, each curve is shifted so that the start month corresponds to its zero lag month on the *x*-axis. The *x*-axis covers 2 years, from January of year(0) to December of year(1). The 0.05 significance level is indicated by the horizontal dashed line.

2.3. Methods

According to Troup (1965), the persistence of the Niño3.4 index can be measured using lagged autocorrelation analysis, which is defined as the correlation of the time series with the time series of a succeeding lag month in a period of given duration (Ding & Li, 2009, 2011). Correlation analysis, linear regression, and composite analysis were also employed in this study.

The significance of these statistical methods was tested using the two-sided Student's *t*-test, where the number of effective degrees of freedom (N^{eff}) was calculated as described by Bretherton et al. (1999):

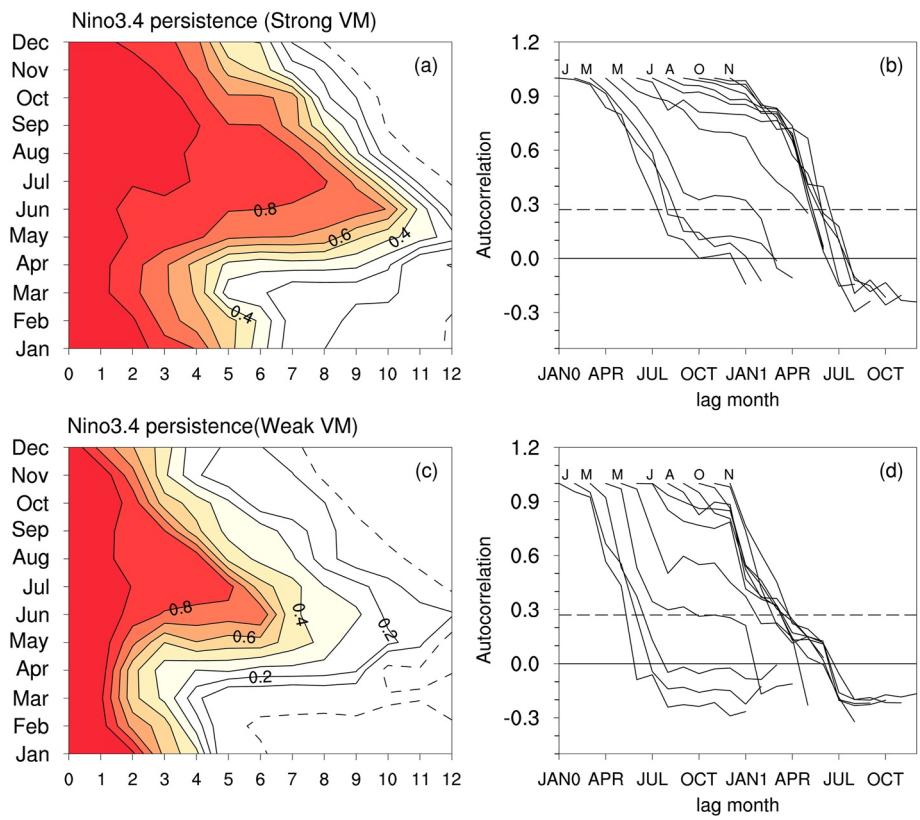

Figure 3. As in Figure 2 but for (a and b) strong VM cases and (c and d) weak VM cases.

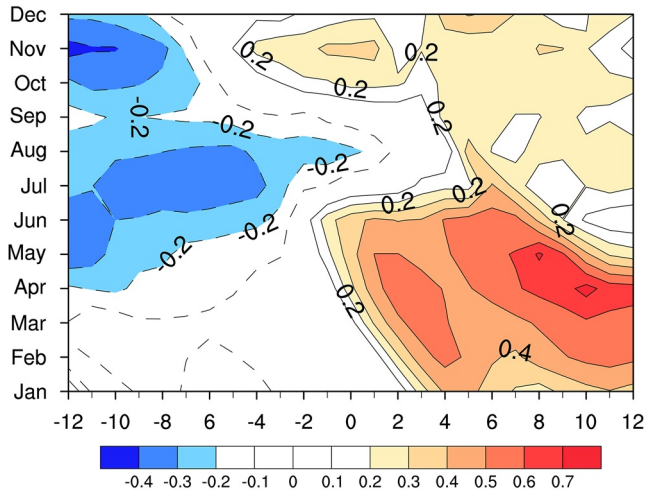

Figure 4. Lead–lag correlations between the area-averaged SSTAs over the Niño3.4 region and the VMI for the period 1950–2020. The VMI from January of year(−1) to December of year(0) is used as the reference to compute the lead–lag correlation coefficients. The contour interval is 0.1; regions of correlation significant at the 0.05 level are shaded.

$$N^{eff} \approx N \frac{1 - r_x r_y}{1 + r_x r_y}$$

where N stands for the amount of effective time steps. The lag-1 autocorrelations of variables x and y is represented by r_x and r_y, respectively. In addition, a bootstrap method was also employed to examine whether a change was statistically significant when we analyzed the outputs from CMIP5 and CMIP6 (Autin & Tu, 2004; Jia et al., 2019).

3. Influence of the VM on the Persistence of ENSO SSTAs

We first examine the seasonal variations of ENSO persistence (Niño3.4 index). According to Webster and Yang (1992), regardless of the starting month, a sharp and obvious decrease (the autocorrelation is reduced to half its original value) signifies the persistence barrier phenomenon of autocorrelations. Figure 2a shows the lagged autocorrelation coefficients of the Niño3.4 index calculated with each starting month (January–December) for the entire period (1950–2020). Note that in Figure 2a the Niño3.4 index starting from March to May has the least persistence (autocorrelation coefficients become insignificant after only 2–3 months), whereas those starting in June–July–August (JJA) tends to have the greatest persistence (autocorrelation coefficients are still significant for leads of 7–9 months), indicating that a persistence barrier occurs in spring (March–May). Figure 2b contains the same information as Figure 2a but is formatted to clearly show the occurrence time of the SPB regardless of the starting month. These results are generally consistent with the findings of Webster and Yang (1992) and Wright (1985).

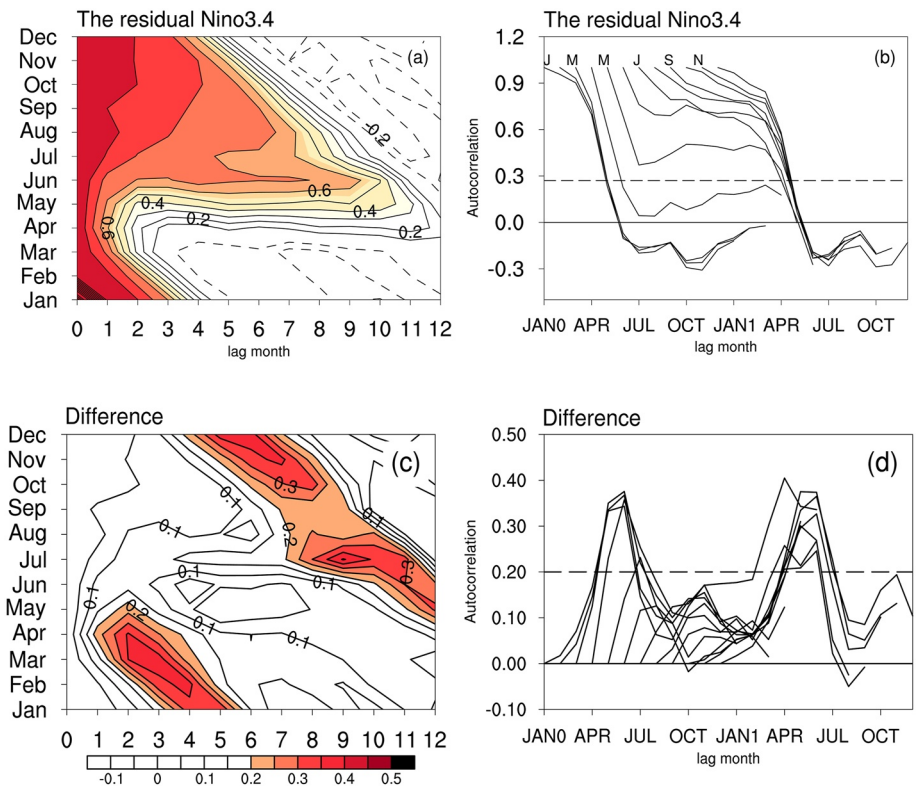

Figure 5. (a, b) As in Figure 2 but for the residual Niño3.4 index. (c) Difference in the autocorrelations obtained from the residual Niño3.4 index and those obtained from the original Niño3.4 index. The contour interval is 0.05. (d) Curves of the differences in the autocorrelations shown in (c) between the original Niño3.4 index and the residual Niño3.4 index.

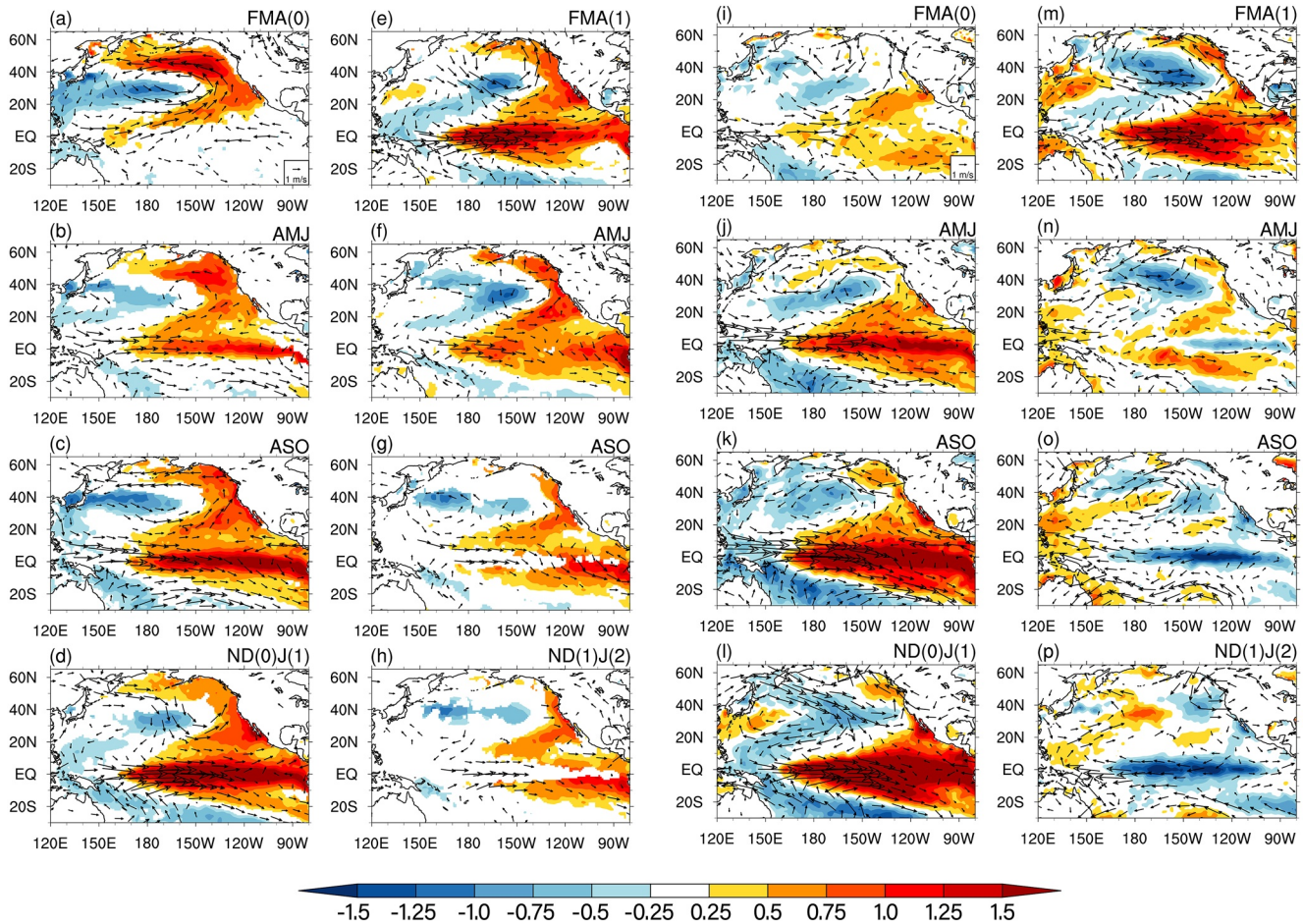

Figure 6. (a–h) Composite differences of the 3-month-averaged SSTAs (°C; shaded) and surface wind velocity (m s^{-1}; vectors) for strong ENSO cases (El Niño event minus La Niña event) co-occurring with strong VM events during ENSO's developing, mature and decaying phases [FMA(0), AMJ, ASO, ND(0)J(1), FMA, MJJ, ASO, ND(1)J(2)]. (i–p) As in (a–h) but for strong ENSO cases (El Niño event minus La Niña event) co-occurring with weak VM events during ENSO's developing, mature and decaying phases [FMA(0), AMJ, ASO, ND(0)J(1), FMA, MJJ, ASO, ND(1)J(2)]. The contour interval of the SSTAs is 0.25°C. The SSTAs and surface wind vectors at the 95% significant level are shown.

To examine the effects of VM events on the persistence of ENSO, firstly, we classify the VM events for all years in the period 1950–2020 into two types according to the intensity of the VMI at its peak phase (FMA; Table 1). An FMA VMI having an intensity >1.0 SD of its 1950–2020 time series defines a strong VM event, and a weak VM event is one in which the 0.0 < VMI <1.0 or 0.0 >VMI>−1.0 SD (Table 1). Figure 3 displays the lagged correlations of the Niño3.4 index during strong and weak VM cases. For strong VM cases (Figure 3a), the Niño3.4 index shows a minimum persistence around March–May. These results suggest that ENSO still shows an SPB phenomenon during strong VM cases. However, the intensity of the SPB for these cases is relatively weak, and the autocorrelation coefficients of the Niño3.4 index show a relatively slow decline and are still significant for lags of 4–5 months during spring (Figure 3b). For weak VM cases (Figure 3c), the lagged autocorrelations of the Niño3.4 index starting from March to May show a rapid decline in April–May, with autocorrelations becoming insignificant after 2–3 months. This rapid decline of autocorrelation during the weak VM cases is much stronger than that during the strong VM cases, implying that the SPB of the Niño3.4 index becomes more distinct (i.e., stronger) during weak VM cases than during strong VM cases.

According to Ding et al. (2015), the VM shows a large variance in FMA and has the greatest correlation with ENSO events in the subsequent winter, so we further calculate the lead–lag correlation between the VMI and Niño3.4 index for the period of 1950–2020. As shown in Figure 4, VMI has a strong lead–lag correlation relationship with the Niño3.4 index throughout the whole year of ENSO cycle, especially in the spring months (February–March–April–May) when the VM leads ENSO by around 11 months (correlation coefficients are

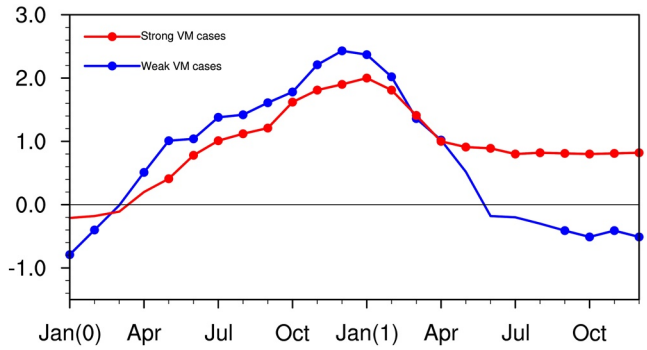

Figure 7. Composite differences in the Niño3.4 index for strong ENSO cases co-occurring with strong (red line) and weak (blue line) VM events in spring during ENSO's developing, mature and decaying phases (from January(0) to December(1)). Markers indicate the values that are statistically significant at the 95% confidence level.

above 0.6). Therefore, to further investigate the influences of VM events on the persistence of ENSO, the preceding VM signal (the VMI; 1949–2019; 12 months) is removed from the original Niño3.4 index (1950–2020) by linear regression, yielding the residual Niño3.4 index. Figures 5a and 5b show the lagged autocorrelations of the residual Niño3.4 index. Note that in Figure 5a the lagged autocorrelations of the residual Niño3.4 index decrease more rapidly in March–May than do those of the original Niño3.4 index (Figure 2a), with correlation coefficients falling below the significance level after only 1–2 months. This suggests that the persistence of the residual Niño3.4 index is substantially different from the original ones that the intensity of SPB becomes much stronger than that obtained from the original Niño3.4 index (Figures 2a and 2b). The differences (Figures 5c and 5d) between the lagged autocorrelations of the original and residual Niño3.4 indices indicate that the autocorrelations of the residual Niño3.4 index lose significance around 1–3 months earlier than the original Niño3.4 index. Moreover, the differences of the autocorrelation coefficients starting from spring (March–May) are reduced by more than 0.3 for lag times of 3–4 months after the VM signal is removed. Thus, we conclude from these results that the VM can enhance the persistence of the ENSO SSTAs (Niño3.4 index) during springtime, and therefore to some extent reduce the intensity of the ENSO SPB (Figures 3, 5c and 5d).

4. Possible Mechanism Linking the VM to the Persistence of ENSO SSTAs

Previous studies have found that VM events can effectively act as an oceanic bridge across which extratropical atmospheric variability in the North Pacific influences ENSO (Bond et al., 2003; Ding et al., 2014). As an SST footprint forced by the previous winter NPO, the VM can trigger the onset of ENSO through the SFM (Vimont, Battisti, & Hirst, 2003; Vimont, Wallace, & Battisti, 2003) or TWC mechanism (Anderson, 2003; Anderson et al., 2013). This section provides some potential mechanism how the VM affects the SPB of ENSO during different VM cases.

Firstly, we begin by inspecting the spatial patterns of 3-month-averaged SSTAs and surface wind anomalies by examining the composite differences in strong ENSO events (El Niño events minus La Niña events) co-occurring with different VM cases (Figure 6). For the strong VM cases (Figures 6a–6h), a VM-like SSTA pattern over the North Pacific peaks in FMA(0). The positive SSTA band in the eastern North Pacific polewards of 20°N associated with the VM extends toward the central equatorial Pacific from spring to summer through the wind–evaporation–SST feedback (Xie & Philander, 1994) in the subtropics (5°–20°N). Therefore, associated with the strong VM events, the warming SSTAs are concentrated in the central equatorial Pacific. Meanwhile, the anomalous westerly winds related to the strong VM events are mostly located over the western equatorial Pacific, rather than in the central–eastern Pacific, as are those for strong ENSO events co-occurring with weak VM cases (Figures 6i–6p). In addition, the intensities of westerly winds during strong VM cases are much weaker than those during weak VM cases (Figure 6). After summer JJA (0), the ocean–atmosphere coupling strengthens the zonal wind and SSTAs along the equator via a positive feedback process (Bjerknes, 1969). During winter ND(0)J(1), approximately 11 months after the VM peaks, the ENSO events enter their mature phase. Note that the positive SSTAs in the equatorial Pacific weaken slowly in the decaying phase of El Niño and do not quickly experience a sign reversal the following spring.

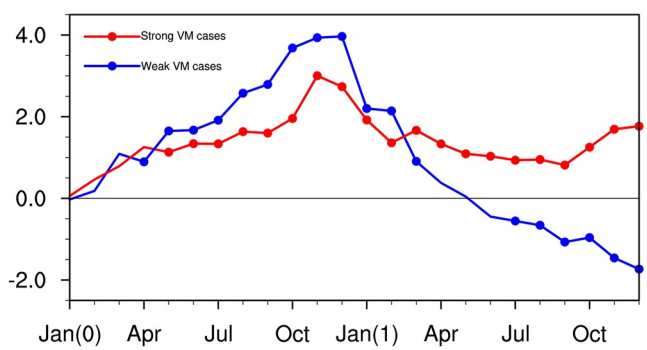

Figure 8. Composite differences in the area-averaged zonal surface wind (m s^{-1}) over the region (5°N–5°S, 150°E–230°W) for strong ENSO cases co-occurring with strong (red line) and weak (blue line) VM events in spring during ENSO's developing, mature and decaying phases (from January(0) to December(1)). Markers indicate the values that are statistically significant at the 95% confidence level.

In contrast, in Figure 6i, there is no significant VM-like SSTA signal from the North Pacific in the composite differences of strong ENSO events co-occurring with weak VM cases. The warm SSTAs in the central–eastern Pacific, possibly arising from the tropical Pacific itself, start to build up around MJJ(0).

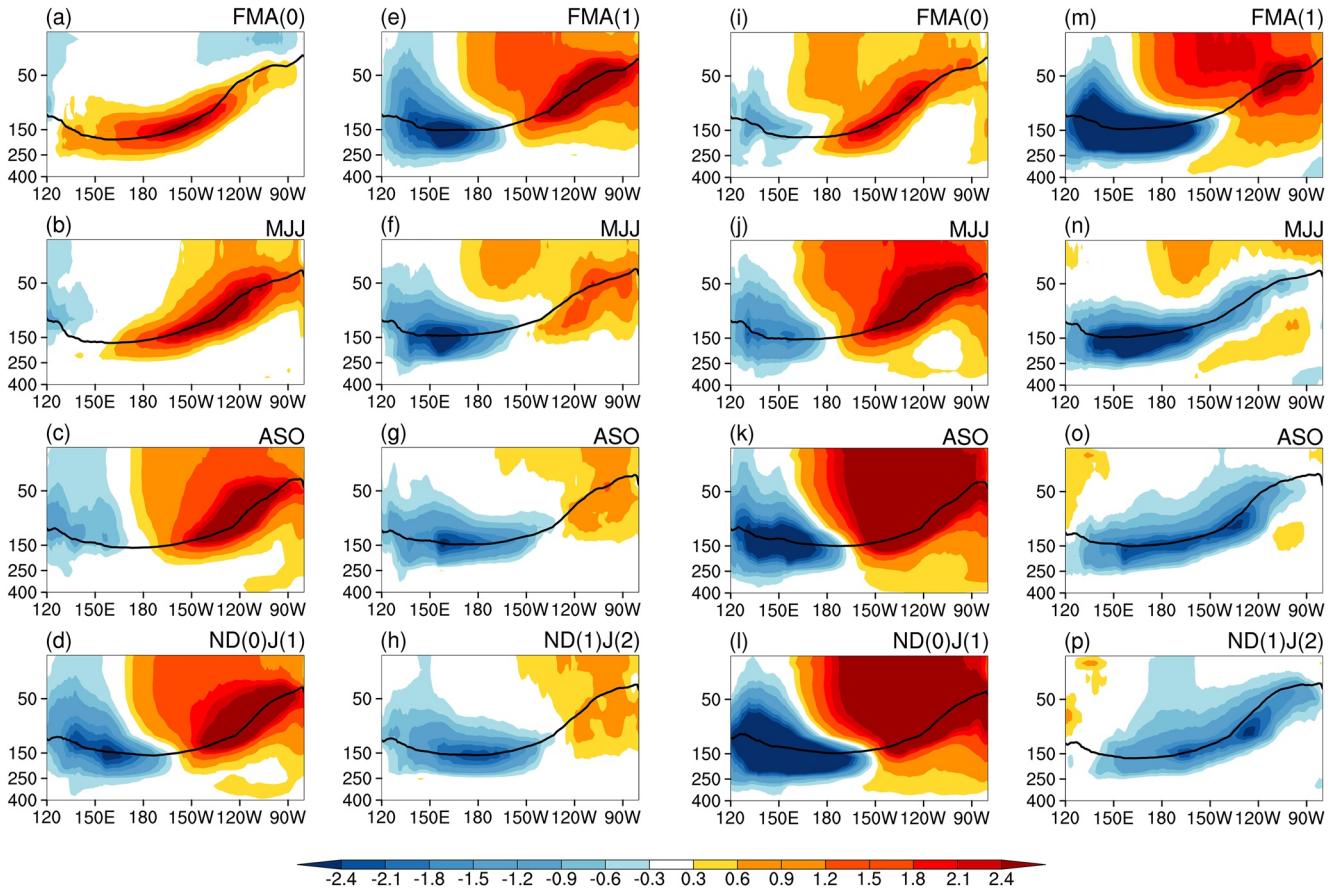

Figure 9. (a–h) Composite differences in the 3-month-averaged ocean subsurface temperature anomalies (°C) at different depths (m) over 5°S–5°N for strong ENSO cases co-occurring with strong VM events (El Niño event minus La Niña event) during ENSO's developing, mature and decaying phases [FMA(0), AMJ, ASO, ND(0)J(1), FMA, MJJ, ASO, ND(1)J(2)]. (i–p) As in (a–h) but for strong ENSO cases (El Niño event minus La Niña event) co-occurring with weak VM events during ENSO's developing, mature and decaying phases [FMA(0), AMJ, ASO, ND(0)J(1), FMA, MJJ, ASO, ND(1)J(2)]. Areas that are significant at the 95% level are shaded. The climatological position of the 22°C isotherm is shown by the black contour.

The intensities of westerly wind anomalies are also associated with the strengthening warm SSTAs throughout the Pacific basin (Figures 6j–6m). Following the peak period of the warm events in boreal winter (ND(0)J(1)), the warm SSTAs decay rapidly and are followed by significantly negative SSTAs in the eastern Pacific (Figure 6n). These results suggest that there are significant differences between the evolution of strong ENSO co-occurring with strong VM events and that of strong ENSO co-occurring with weak VM events (the typical ENSO cycle); namely, the positive SSTAs of strong ENSO co-occurring with strong VM events may develop and decay more slowly and have no sign reversal in the decaying phase of ENSO, thereby allowing the SSTAs of ENSO to persist much longer, which indicates a weak SPB phenomenon in the strong VM cases but a relatively strong SPB phenomenon in the weak VM cases.

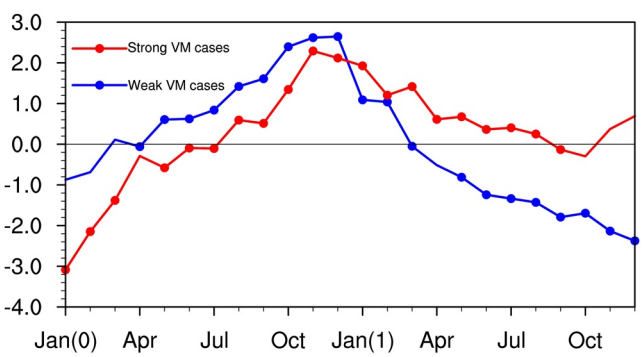

Figure 10. Composite differences evolution of the normalized warm water volume (WWV) for strong ENSO cases co-occurring with strong (red line) and weak (blue line) VM events in spring during ENSO's developing, mature and decaying phases (from January(0) to December(1)). Markers indicate the values that are statistically significant at the 95% confidence level.

Next, we discuss in detail the evolution of the Niño3.4 index for different VM cases. We first show the composite differences in the Niño3.4 index for the 13 strong El Niño events minus the 10 strong La Niña events listed in Table 1 (Figure 7). From Figure 7, it is notable that El Niño (La Niña) events tend to experience a sign reversal from positive to negative (negative to positive) in spring, reach their maximum intensity the following winter, and then decay rapidly across the zero-anomaly line again in spring of the next year. These results are consistent with Webster and Yang (1992). The sign reversal of SSTAs signifies a rapid decline in the persistence of the Niño3.4 index, which

Table 2
Basic Information of the CMIP5 and CMIP6 Models Used in This Study

CMIP5 models			
		Resolution (lon × lat)	
Model ID	Institute ID and Country	Atmosphere	Ocean
BCC-CSM1-1-m	BCC/China	320 × 160	360 × 232
CanESM2	CCCma/Canada	128 × 64	256 × 192
CCSM4	NCAR/United States	288 × 192	320 × 384
CESM1-BGC	NSF-DOE-NCAR/United States	288 × 192	320 × 384
CESM1-CAM5	NSF-DOE-NCAR/United States	288 × 192	320 × 384
CESM1-FASTCHEM	NSF-DOE-NCAR/United States	288 × 192	320 × 384
CMCC-CMS	CMCC/Italy	192 × 96	182 × 149
GFDL-ESM2G	NOAA-GFDL/United States	144 × 90	360 × 210
GISS-E2-R	NASA-GISS/United States	144 × 90	144 × 90
MIROC5	MIROC/Japan	256 × 128	256 × 224
NorESM1-M	NCC/Norway	144 × 96	320 × 384
NorESM1-ME	NCC/Norway	144 × 96	320 × 384
CMIP6 models			
		Resolution (lon × lat)	
Model ID	Institute ID and Country	Atmosphere	Ocean
AWI-CM-1-1-MR	AWI/Germany	unstructured grid	unstructured grid
BCC-CSM2-MR	BCC/China	320 × 160	360 × 232
CAMS-CSM1-0	CAMS/China	320 × 160	360 × 200
CAS-ESM2-0	CAS/China	256 × 128	360 × 196
CESM2-WACCM-FV2	NCAR/United States	144 × 96	320 × 384
CESM2	NCAR/United States	288 × 192	320 × 384
CIESM	THU/China	288 × 192	320 × 384
CMCC-CM2-SR5	CMCC/Italy	288 × 192	362 × 292
CanESM5	CCCma/Canada	128 × 64	360 × 291
E3SM-1-1-ECA	E3SM-Project/United States	360 × 180	360 × 180
EC-Earth3-LR	EC-Earth-Consortium/Europe	320 × 160	362 × 292
E3SM-1-1	E3SM-Project/United States	360 × 180	360 × 180
EC-Earth3-Veg-LR	EC-Earth-Consortium/Europe	320 × 160	362 × 292
EC-Earth3-Veg	EC-Earth-Consortium/Europe	512 × 256	362 × 292
FGOALS-g3	CAS/China	180 × 80	360 × 218
GISS-E2-2-G	NASA-GISS/United States	144 × 90	144 × 90
HadGEM3-GC31-LL	MOHC/United Kingdom	192 × 144	360 × 330
IITM-ESM	CCCR-IITM/India	192 × 94	360 × 200
MRI-ESM2-0	MRI/Japan	320 × 160	360 × 363
SAM0-UNICON	SNU/Korea	288 × 192	320 × 384

favors the occurrence of a persistence barrier. The ENSO SPB coincides with this sign reversal in the Niño3.4 index, indicating a close connection between these two phenomena. The composite difference in the Niño3.4 index for strong VM cases (11 strong positive VM events minus 8 strong negative VM events) is shown in Figure 7. Note that the Niño3.4 index for strong VM cases reverses from negative to positive during spring, peaks the following winter, and decreases slowly, but with no sign reversal in spring of the next year. The composite difference for weak

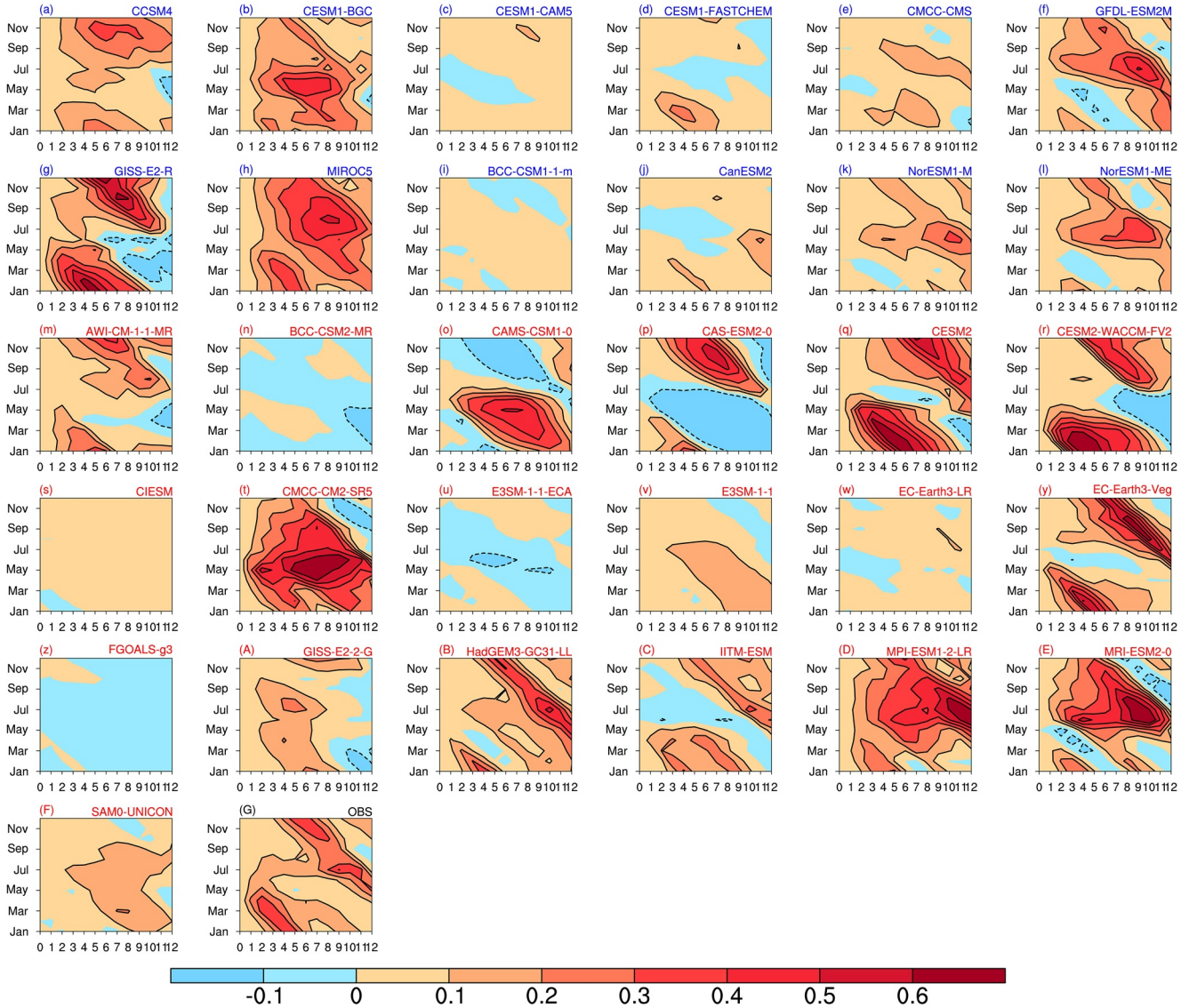

Figure 11. Lagged autocorrelations (shading at the 95% significance level; ≥0.27) of Niño3.4 index (the area-averaged SSTAs over 5°S–5°N, 170°–120°W) from the CMIP5 outputs. (m–F) Same as (a–l), but for the Niño3.4 index from the CMIP6 outputs. (G) Same as (a–l), but for the observed Niño3.4 index. The contour interval is 0.1.

VM cases (6 weak positive VM events minus 7 weak negative VM events) shows composite SSTAs of very small amplitude (smaller than 0.5). However, it also undergoes a sign reversal in spring of the next year, which may be related to a relatively strong SPB of ENSO. These results indicate that the positive SSTAs of ENSO decay slowly and persist longer in the following year during strong VM cases, which may be why the intensity of the SPB for the strong VM cases is reduced. No phase reversal the next spring means that the autocorrelation coefficients of the Niño3.4 index starting from March–May can persist much longer than those during weak VM events. These results indicate that the SSTAs of ENSO events co-occurring with strong VM events develop (decay) slowly and do not undergo a sign reversal in spring of the year(1), suggesting that may be an important reason why the ENSO SPB in spring is weak during strong VM cases while relatively strong during weak VM cases.

In addition, we further investigate the area-averaged westerly winds located over the western Pacific (5°S–5°N, 150°E–230°W) for ENSO co-occurring with strong and weak VM events (Figure 8). From Figure 8, we note that the intensities of the area-averaged westerly winds during strong VM cases are relatively weaker than those associated with weak VM events. Previous studies have found that such relatively weak westerly winds, the Bjerknes feedback (Bjerknes, 1969) can be disrupted by weak equatorial convection anomalies, and thus the warm

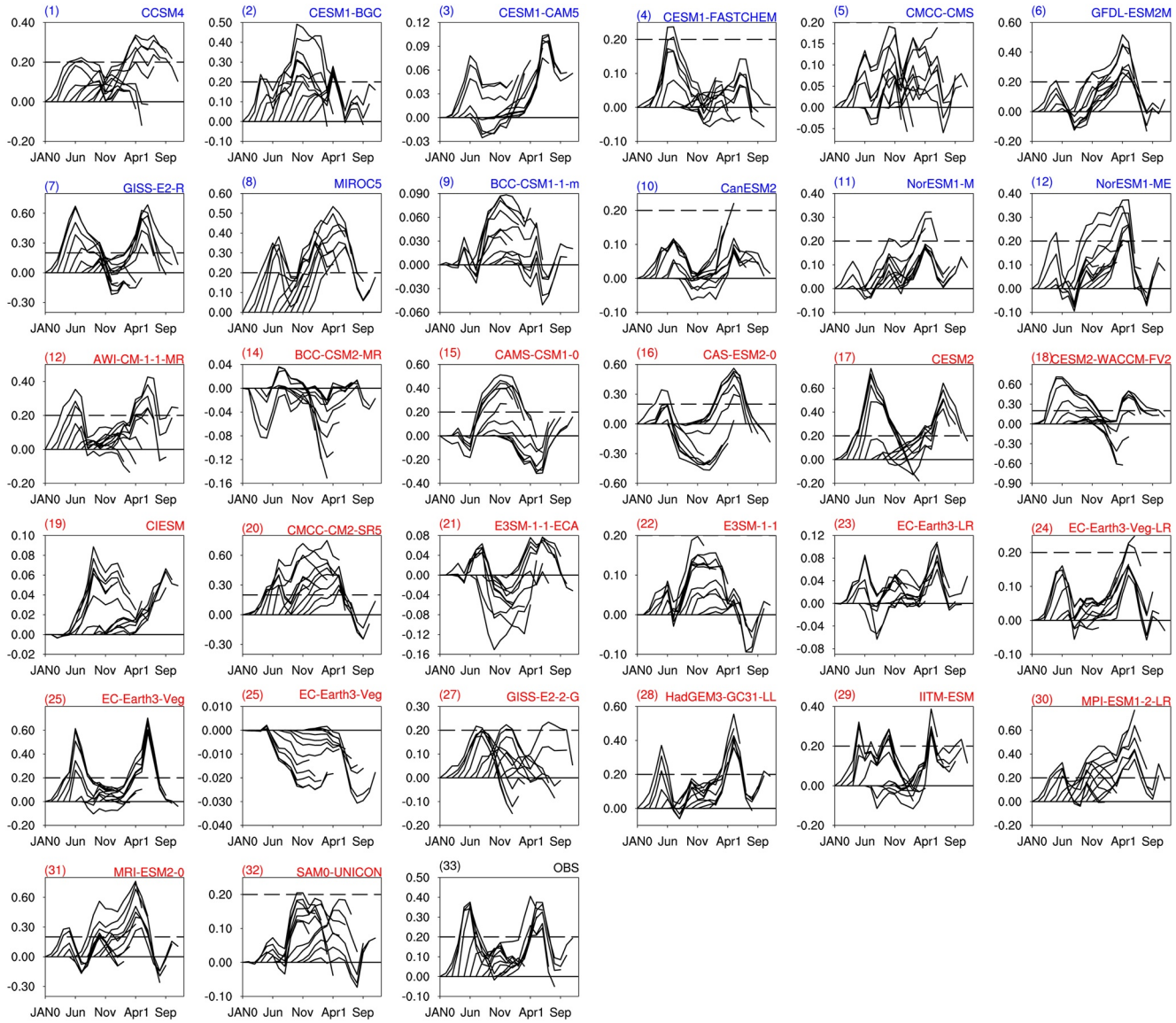

Figure 12. (1–32) Autocorrelation curves of the Niño3.4 index for each of the 12 starting months shown in Figure 10 (a–g) as a function of time. For clarity, each curve is shifted so that the start month corresponds to its zero-lag month on the *x*-axis. The *x*-axis covers 2 years, from January of year(0) to December of year(1).

subsurface anomalies are not fully recharged before winter D(0)JF(1) (Clarke et al., 2007; Jin, 1997; Lee et al., 2020). This means that the El Niño event is not as fully developed during this period as in a typical ENSO cycle. Thus, after El Niño peaks in winter D(0)JF(1), we find that the westerly winds over the western–central Pacific are almost weak throughout the ENSO cycle, which indicates that the subsurface water is discharged/recharged slowly in the developing and decaying phase of ENSO events. As a result, the ENSO SSTAs during strong VM cases appear (disappear) slowly during springtime and do not experience a phase reversal from positive (negative) to negative (positive) SSTAs during their decayed phase, indicating that the ENSO events can persist much longer than those during the weak VM cases. In other words, there will be a weak (strong) SPB of ENSO occurring in spring during strong (weak) VM cases.

To further explain the evolution of the subsurface temperature anomalies for ENSO associated with different VM cases, we show the detailed evolution of 3-month—averaged subsurface temperature anomalies for strong ENSO events associated with different VM cases. For strong VM cases (Figures 9a–9h), the subsurface temperature anomalies propagate slowly toward the surface over the central–eastern Pacific in year(0). At the same

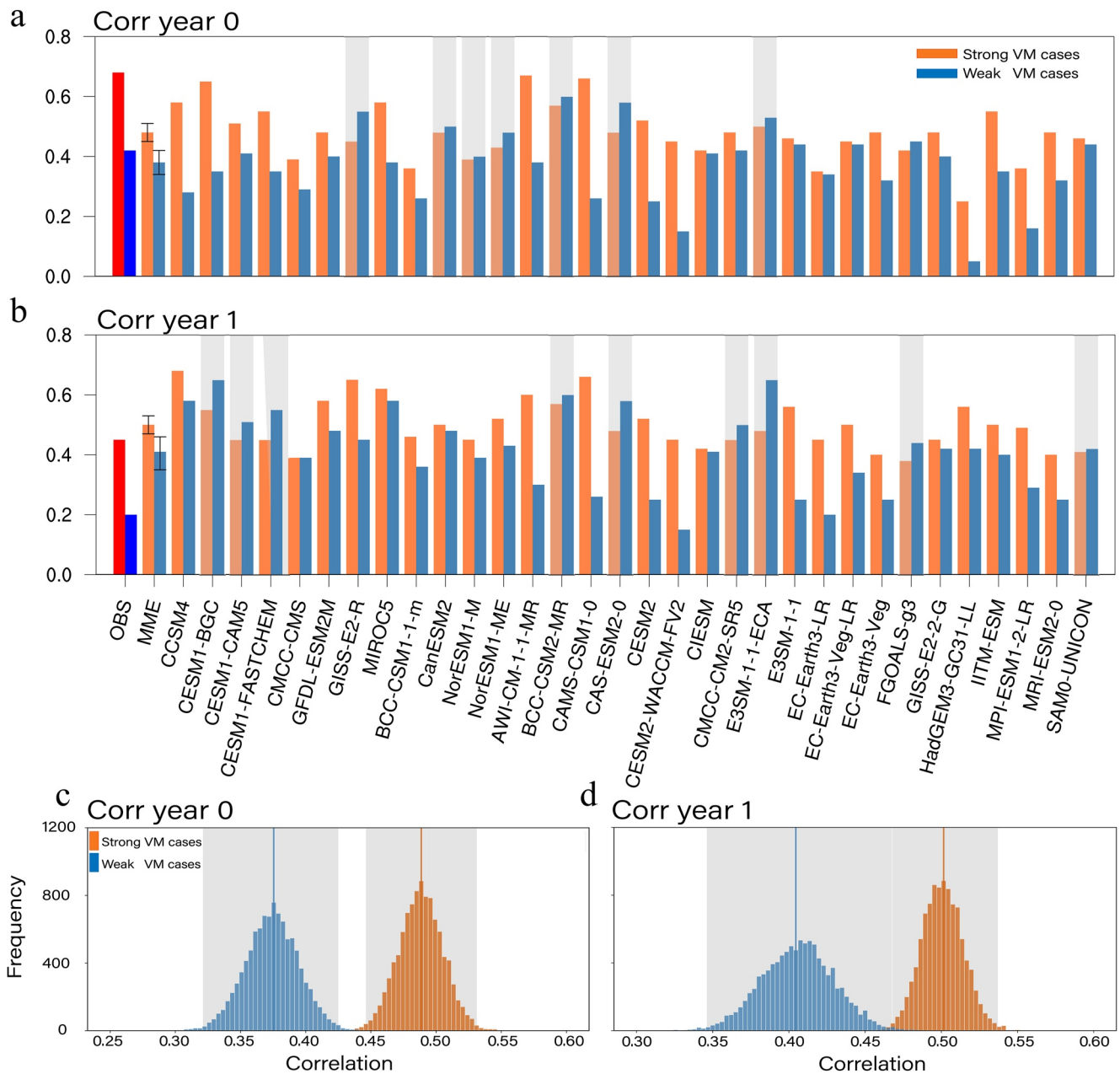

Figure 13. (a, b) The FMA-averaged lagged autocorrelations of the original Niño3.4 index (orange bars) and residual Niño3.4 index (blue bars) in individual CMIP models and their MME mean during year(0) and year(1), respectively (error bars of the MME means are calculated as 2 SDs of a total of 10,000 inter-realizations of a bootstrap method). The red and blue bars represent the results from observations. (c–d) Histograms of 10,000 realizations of a bootstrap method for the differences in (a) and (b), respectively. The blue and orange vertical lines indicate the mean values of 10,000 inter-realizations for the SSTA differences between the FMA-averaged lagged autocorrelations of the original Niño3.4 index (orange bars) and residual Niño3.4 index (blue bars), respectively. The gray shaded regions represent the 1% and 99% percentiles of the 10,000 inter-realizations. The orange and blue vertical lines indicate the mean values of 10,000 inter-realizations for these two different cases, respectively.

time, the subsurface temperature anomalies remain anomalously deep in DJF(0) during this case. These results may suggest that the recharging/discharging process is weak and slow in springtime. In contrast, Figures 9i–9q show that the warm subsurface anomalies in weak VM cases become fully and quickly charged in DJF(0), which permits that the ENSO events to enter their mature phase. After El Niño peaks in DJF(0), the warm subsurface anomalies are discharged quickly and are replaced by cold subsurface anomalies in JJA(1) by the strong anomalous westerlies (Figure 8), indicating that a phase reversal occurs (from an El Niño event to a La Niña event)

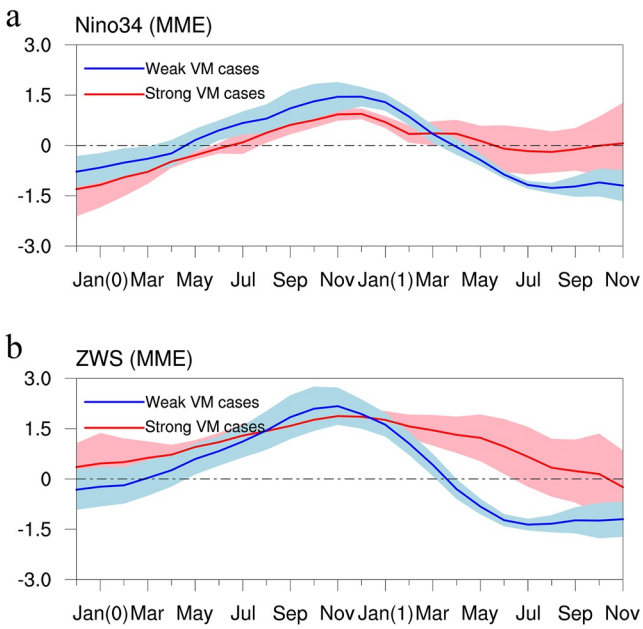

Figure 14. (a) Temporal evolution of the Niño3.4 index during the developing(0) and decaying(0) years from CMIP5 and CMIP6. (b) As in (a) but for the monthly averaged zonal surface wind (m s^{-1}) over the region (5°N–5°S, 150°E–230°W). The red and blue lines represent the MME evolutions of the Niño3.4 index and the MME evolutions of the zonal wind stress for the strong VM cases and weak VM cases, respectively. In (a) and (b), the gray shading indicates the interquartile range between the 25th and 75th percentiles.

during this period. In addition, we calculated the warm water volume (WWV; defined as the averaged depth of 20°C over 120°E–80°W, 5°S–5°N) to verify the evolution of these strong (weak) and fast (slow) recharge/discharge processes during these two different VM cases (Figure 10). From Figure 10, we note that the WWV transits from positive WWV (recharge) to negative WWV (discharge) in the period FMA(0) to ND(1)J(2), which through the so-called tilt mode (west-east heat/mass transition). Namely,during the weak VM cases, the WWV is quickly charged and quickly discharged at the development and decayed phase of ENSO events. However, the WWV are relatively small and slowly recharged (discharged) at the development (decayed) phase of ENSO events during the strong VM cases (Clarke, 2010; Kumar & Hu, 2014). These results indicate that the different propagation of the warm subsurface temperature anomalies may be another possible reason why VM influent the ENSO SPB.

5. CMIP5 and CMIP6 Multimodel Outputs

To further confirm the influence of VM on the persistence of ENSO SSTAs, we analyze the outputs of the CMIP5 and CMIP6 preindustrial simulations. According to the findings of Wang et al. (2021), we selected 32 models (12 CMIP5 and 20 CMIP6 models) that can successfully reproduce the relationship between the VM and subsequently ENSO (see their Figures 7 and 8). Detailed information on these 32 CMIP models used in this study is listed in Table 2. Figures 11a–11f show the differences in lagged autocorrelations between the Niño3.4 index and residual Niño3.4 index as calculated with the CMIP5 and CMIP6 outputs. Results show that a total of 24 of 32 CMIP5 and CMIP6 models (or 75%) simulate decreased autocorrelations of the residual Niño3.4 index. Figure 12(1–32) contains the same information as Figures 10a–10f but is formatted to clearly show the occurrence time of the SPB regardless of the starting month, especially during springtime. The results of most models are consistent with the observations (Figure 11g and Figure 12(33)).

In addition, we use the averaged correlation coefficient of the Niño3.4 index starting from March to May which becomes insignificant after only 2–3 months to further evaluate the intensity of the ENSO SPB during strong and weak VM cases. A larger proportion of the CMIP5 and CMIP6 models (26 of 32 models, or 81.25%) reproduce higher correlation coefficients during strong VM cases than those during weak VM cases (Figure 13a). The multimodel mean of the correlation coefficients in these 32 models is also much greater during strong VM cases than during weak VM cases, which is close to the observed result and statistically significant above the 95% confidence level (Figure 13c) according to a bootstrap method (Austin & Tu, 2004; Jia et al., 2019). Likewise, a total of 23 of 32 (or 71.88%) models also simulate higher correlation coefficients of Niño3.4 index in the spring of year (1) during strong VM cases than those during weak VM cases (Figure 13b). Furthermore, the multimodel ensemble (MME) of the 32 models also simulates a greater correlation coefficient during strong VM cases than during weak VM cases in the spring of year (1), again statistically significant above the 95% confidence level (Figure 13d).

The results presented above indicate that the CMIP5 and CMIP6 models capture well the influence of the previous spring VM variability on the intensity of the ENSO SPB, which is consistent with the observed results. Next, we use the MME of these models to analyze the evolution of the Niño3.4 index and zonal wind anomalies for strong and weak VM cases during developing and decaying years of ENSO, respectively. In Figure 14a, the evolution of the Niño3.4 index undergoes a sign reversal in May(0) of the developing year and can then persist for a long time until June(1) for strong VM cases, whereas it experiences sign reversals in both the developing and decaying years of ENSO for weak VM cases. Meanwhile, the evolutions of the zonal wind anomalies during these two cases are generally similar to the evolutions of the Niño3.4 index, except that the sign reversal is about one month ahead. These results indicate that the intensity of the ENSO SPB is weaker for strong VM cases than it is for weak VM cases, which again verifies our conclusions analyzed by observations.

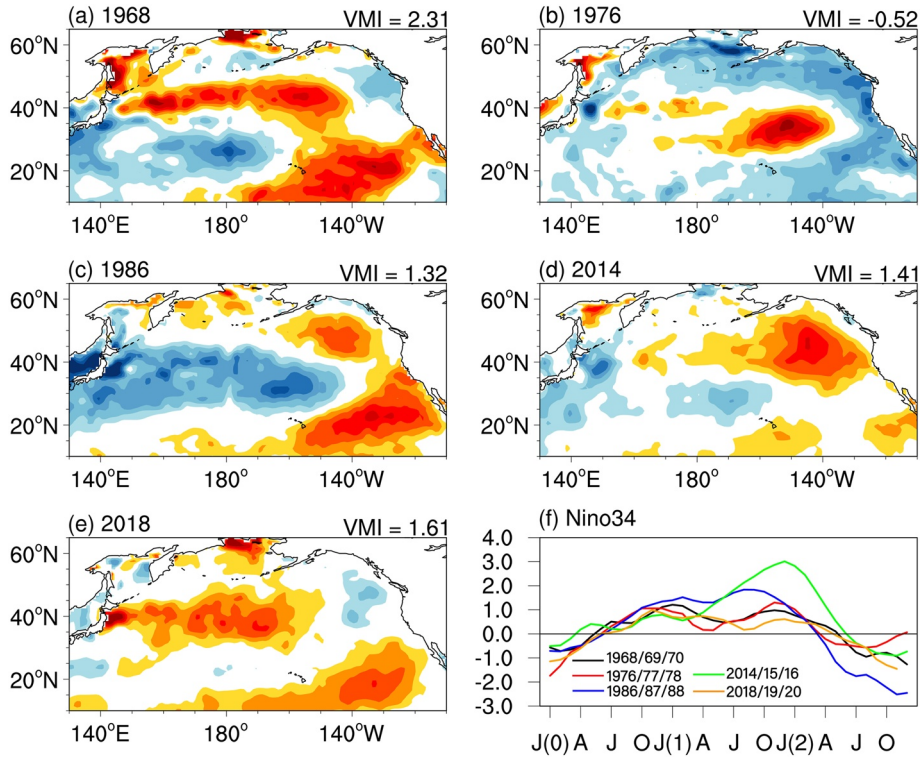

Figure 15. Two-winter ENSO events. (a–e) the FMA-averaged SSTAs (°C; shaded): (a) 1968, (b) 1976, (c) 1986, (d) 2014, and (e) 2018. The contour interval of the SSTAs is 0.25°C. The FMA VMI for the first year of these five two-winter El Niño events are 2.31, −0.51, 1.32, 1.41, and 1.61, respectively. (f) The evolution of the Niño3.4 index during these five two-winter El Niño events: 1968/69/70 (black line), 1976/77/78 (red line), 1986/87/88 (blue line), 2014/15/16 (green line), and 2018/19/20 (orange line), respectively.

6. Summary and Discussion

This study provided a detailed investigation about the influence of the VM on the persistence of the ENSO SSTAs. Our analyses show that the VM can enhance the persistence of ENSO SSTAs and reduce the intensity of the spring persistence barrier (SPB) of ENSO SSTAs. The intensity of the ENSO SPB is weak for strong VM cases but relatively strong for weak VM cases. For strong ENSO cases co-occurring with strong VM events, the SSTAs of ENSO decay slowly during their decaying phase and do not experience a sign reversal in spring of the next year, resulting in a weak SPB of ENSO occurring in spring of the next year. In contrast, for weak VM cases, although the Niño3.4 index experience a similar evolution to those for strong VM cases, it develops rapidly and reaches a greater amplitude during developing year. After they peak in winter, the Niño3.4 index undergoes a rapid sign reversal in spring of the year(1), indicating that relatively strong ENSO SPB occurs in the spring of these cases.

Furthermore, the VM can affect the strength of the westerly winds over the western Pacific. We found that the westerly winds increase rapidly during development phase of ENSO, and become very strong in mature phase. After the mature phase, these events decay rapidly for strong VM cases. However, they show a relatively slow and weak increase during their development and mature phases. After the mature phase, they can persist much longer with no sign reversal for strong weak VM cases. In addition to the different evolutions of the SSTAs and sea surface wind during these two cases, the warm (cold) subsurface temperature anomalies propagate more slowly during strong VM cases than those during weak VM cases, indicating that the strength of recharge/discharge oscillation is weak during the strong VM cases but relatively weak during weak VM cases. In addition, the results mentioned above are also consistent with Hu et al. (2019), when VM is stronger, the SNR is larger, then the persistence of SSTAs is longer and SPB is weaker.

Most of selected CMIP5 and CMIP6 model simulations confirm that the VM can significantly affect the intensity of the ENSO SPB. Compared with the original Niño3.4 index, a total of 24 of 32 CMIP5 and CMIP6 models (or 75%) simulate decreased autocorrelations of the residual Niño3.4 index. Furthermore, results also show that about 81.25% (26 out of 32) and 71.88% (23 out of 32) CMIP5 and CMIP6 models can simulate greater correlation coefficients and longer persistence in springtime of developing and decaying phases of ENSO events during strong VM cases than those during weak VM cases. The MME of these model simulations also indicates that our results derived from observations are reliable.

In addition, our work also finds that a new type of El Niño event known as "two-winter El Niño" (including five events in 1968/69/70, 1976/77/78, 1986/87/88, 2014/15/16, and 2018/19/20) are closely related to a preceding strong VM signal, except the 1976/77/78 event is preceded by a weak negative VM event in spring of the first year of the two consecutive years of these prolonged El Niño events (Figure 15). This may provide additional evidence for why strong VM events can cause ENSO SSTAs to persist for much longer than weak VM events.

It is important to note that while our results highlight the effect of the North Pacific VM on the ENSO SST persistence, we cannot neglect the variabilities from other oceans. For example, the 1997/98 super El Niño event, its SSTAs declined rapidly and undergone a sign reversal in the spring of its decaying year even though a strong positive VM event (VMI = 1.05) occurred in the spring of 1997. This implies that we should also consider the roles of variabilities from other oceans (the Indian Ocean dipole; the South Pacific Quadrapole and the North American dipole; Ding et al., 2014, 2016, 2017; Saji et al., 1999). In addition, this work only investigated the influence of the variation from the North Pacific (e.g., VM) on the tropics (ENSO), the impacts of ENSO on the North Pacific via Pacific–North American pattern have not considered yet (Li et al., 2019; Wallace & Gutzler, 1981). The interactions among these processes as well as their relative contributions need to be further examined.

Data Availability Statement

The SST data is available at https://climatedataguide.ucar.edu/climate-data/sst-data-hadisst-v11 (Rayner, 2003). The subsurface ocean temperature data set is available at http://www.ocean.iap.ac.cn/pages/dataService/ (Cheng et al., 2017) [Data set]. The data set of atmospheric fields can be download at https://www.esrl.noaa.gov/psd/data/gridded/data.ncep.reanalysis.html (Kalnay et al., 1996) [Data set]. The CMIP data sets (Eyring et al., 2016; Taylor et al., 2012) used in this study are available through the websites https://esgf-node.llnl.gov/search/cmip5/ and https://esgf-node.llnl.gov/search/cmip6/ [Data set].

Acknowledgments
The authors wish to thank three anonymous reviewers for helpful comments and suggestions. This research was jointly supported by the National Natural Science Foundation of China (41975070 and 41975076).

References

An, S. I., & Wang, B. (2005). The forced and intrinsic low-frequency modes in the North Pacific. *Journal of Climate*, *18*(6), 876–885. https://doi.org/10.1175/JCLI-3298.1

Anderson, B. T. (2003). Tropical Pacific sea-surface temperatures and preceding sea level pressure anomalies in the subtropical North Pacific. *Geophysical Research Letters*, *108*, D324732. https://doi.org/10.1029/2003JD003805

Anderson, B. T., Perez, R. C., & Karspeck, A. (2013). Triggering of El Niño onset through trade wind-induced charging of the equatorial Pacific. *Geophysical Research Letters*, *40*, 1212–1216. https://doi.org/10.1002/grl.50200

Ashok, K., Behera, S. K., Rao, S. A., Weng, H., & Yamagata, T. (2007). El Niño Modoki and its possible teleconnection. *Geophysical Research Letters*, *112*. https://doi.org/10.1029/2006jc003798

Austin, P. C., & Tu, J. V. (2004). Bootstrap methods for developing predictive models. *The American Statistician*, *58*, 131–137. https://doi.org/10.1198/0003130043277

Ballester, J., Rodríguez-Arias, M. À., & Rodó, X. (2011). A new extratropical tracer describing the role of the Western Pacific in the onset of El Niño: Implications for ENSO understanding and forecasting. *Journal of Climate*, *24*, 1425–1437. https://doi.org/10.1175/2010JCLI3619.1

Barnston, A. G., Tippett, M. K., Ranganathan, M., & L'Heureux, M. L. (2017). Deterministic skill of ENSO predictions from the North American Multimodel Ensemble. *Climate Dynamics*, *53*, 7215–7234. https://doi.org/10.1007/s00382-017-3603-3

Bjerknes, J. (1969). Atmospheric teleconnections from the equatorial Pacific. *Monthly Weather Review*, *97*, 163–172. https://doi.org/10.1175/1520-0493(1969)097<0163:atftep>2.3.co;2

Blumenthal, M. B. (1991). Predictability of a coupled ocean–atmosphere model. *Journal of Climate*, *4*, 766–784.

Bond, N. A., Overland, J. E., Spillane, M., & Stabeno, P. (2003). Recent shifts in the state of the North Pacific. *Geophysical Research Letters*, *30*, 2183. https://doi.org/10.1029/2003GL018597

Bretherton, C. S., Widmann, M., Dymnikov, V. P., Wallace, J. M., & Bladé, I. (1999). The effective number of spatial degrees of freedom of a time-varying field. *Journal of Climate*, 1990–2009. https://doi.org/10.1175/1520-0442(1999)012<1990:tenosd>2.0.co;2

Chen, D., Lian, D., Fu, C., Cane, M. A., Tang, Y., Murtugudde, R., et al. (2015). Strong influence of westerly wind bursts on El Niño diversity. *Nature Geoscience*, *8*, 339–345. https://doi.org/10.1038/ngeo2399

Chen, M., Yu, J. Y., Wang, X., & Chen, S. (2021). Distinct onset mechanisms of two subtypes of CP El Niño and their changes in future warming. *Geophysical Research Letters*, *48*. https://doi.org/10.1029/2021GL093707

Cheng, L., Trenberth, K., Fasullo, J., Boyer, T., Abraham, J., & Zhu, J. (2017). Improved estimates of ocean heat content from 1960 to 2015 [Data set]. , *3*, e1601545. https://doi.org/10.1126/sciadv.1601545

Cheng, L., & Zhu, J. (2016). Benefits of CMIP5 multimodel ensemble in reconstructing historical ocean subsurface temperature variation. *Journal of Climate*, *29*(15), 5393–5416. https://doi.org/10.1175/JCLI-D-15-0730.1

Clarke, A. J. (2010). Analytical theory for the quasi-steady and low-frequency equatorial ocean response to wind forcing: The 'tilt' and 'warm water volume' modes. *Journal of Physical Oceanography*, *40*(1), 121–137. https://doi.org/10.1175/2009JPO4263.1

Clarke, A. J., & Van Gorder, S. (1999). The connection between the boreal spring southern oscillation persistence barrier and biennial variability. *Journal of Climate*, *12*, 610–620. https://doi.org/10.1175/1520-0442(1999)012<0610:tcbtbs>2.0.co;2

Clarke, A. J., Van Gorder, S., & Colantuono, G. (2007). Wind stress curl and ENSO discharge/recharge in the equatorial pacific. *Journal of Physical Oceanography*, *37*(4), 1077–1091. https://doi.org/10.1175/JPO3035.1

Dai, A., Trenberth, K. E., & Karl, T. R. (1998). Global variations in droughts and wet spells: 1900–1995. *Geophysical Research Letters*, *25*(17), 3367–3370. https://doi.org/10.1029/98GL52511

Ding, R. Q., & Li, J. (2009). Long-term trend and decadal variability of persistence of daily 500 mb geopotential height anomalies during boreal winter. *Monthly Weather Review*, *137*, 3519–3534. https://doi.org/10.1175/2009MWR2841.1

Ding, R. Q., & Li, J. (2011). Winter persistence barrier of sea surface temperature in the northern tropical Atlantic associated with ENSO. *Journal of Climate*, *24*, 2285–2299. https://doi.org/10.1175/2011JCLI3784.1

Ding, R., Li, J., & Tseng, Y. H. (2014). The impact of South Pacific extratropical forcing on ENSO and comparisons with the North Pacific. *Climate Dynamics*, *44*, 2017–2034. https://doi.org/10.1007/s00382-014-2303-5

Ding, R., Li, J., Tseng, Y. H., Sun, C., & Guo, Y. (2015). The Victoria mode in the North Pacific linking extratropical sea level pressure variations to ENSO. *Journal of Geophysical Research: Atmospheres*, *120*, 27–45. https://doi.org/10.1002/2014jd022221

Ding, R., Li, J., Tseng, Y. H., Sun, C., & Zheng, F. (2016). Linking a sea level pressure anomaly dipole over North America to the central Pacific El Niño. *Climate Dynamics*, *49*, 1321–1339. https://doi.org/10.1007/s00382-016-3389-8

Ding, R., Li, J., Tseng, Y. H., Sun, C., & Zheng, F. (2017). Linking a sea level pressure anomaly dipole over North America to the central Pacific El Niño. *Climate Dynamics*, *49*(4), 1321–1339. https://doi.org/10.1007/s00382-016-3389-8

Duan, W., Liu, X., Zhu, K., & Mu, M. (2009). Exploring the initial errors that cause a significant "spring predictability barrier" for El Niño events. *Geophysical Research Letters*, *114*. https://doi.org/10.1029/2008jc004925

Eyring, V., Bony, S., Meehl, G. A., Senior, C. A., Stevens, B., Stouffer, R. J., & Taylor, K. E. (2016). Overview of the Coupled Model Intercomparison Project Phase 6 (CMIP6) experimental design and organization [Data set]. , *9*(5), 1937–1958. https://doi.org/10.5194/gmd-9-1937-2016

Foltz, G. R., & Mcphaden, M. J. (2006). The role of oceanic heat advection in the evolution of tropical north and south atlantic sst anomalies. *Journal of Climate*, *19*(23), 6122–6138. https://doi.org/10.1175/JCLI3961.1

Ham, Y. G., Kug, J. S., Park, J. Y., & Jin, F. F. (2013). Sea surface temperature in the north tropical Atlantic as a trigger for El Niño/Southern Oscillation events. *Nature Geoscience*, *6*(2), 112–116. https://doi.org/10.1038/ngeo1686

Hu, Z. Z., Kumar, A., Huang, B., Zhu, J., & Guan, Y. (2014). Prediction skill of North Pacific variability in NCEP Climate Forecast System Version 2: Impact of ENSO and beyond. *Journal of Climate*, *27*(11), 4263–4272. https://doi.org/10.1175/JCLI-D-13-00633.1

Hu, Z. Z., Kumar, A., Zhu, J., Peng, P., & Huang, B. (2019). On the challenge for ENSO cycle prediction: An example from NCEP Climate Forecast System, version 2. *Journal of Climate*, *32*(1), 183–194. https://doi.org/10.1175/JCLI-D-18-0285.1

Jia, F., Cai, W., Wu, L., Gan, B., Wang, G., Kucharski, F., et al. (2019). Weakening Atlantic Niño–Pacific connection under greenhouse warming. *Science Advance*, *5*, eaax4111.

Jin, D., & Kirtman, B. P. (2009). Why the Southern Hemisphere ENSO responses lead ENSO. *Journal of Geophysical Research: Atmospheres*, *114*. https://doi.org/10.1029/2009jd012657

Jin, E. K., Coauthors, J. L., Wang, B., Park, C.-K., Kang, I.-S., Kirtman, B. P., et al. (2008). Current status of ENSO prediction skill in coupled ocean–atmosphere models. *Climate Dynamics*, *31*, 647–664. https://doi.org/10.1007/s00382-008-0397-3

Jin, F. F. (1997). An equatorial ocean recharge paradigm for ENSO. Part I: Conceptual model. *Journal of the Atmospheric Sciences*, 811–829. https://doi.org/10.1175/1520-0469(1997)054<0811:aeorpf>2.0.co;2

Kalnay, E., Kanamitsu, M., Kistler, R., Collins, W., Deaven, D., Gandin, L., et al. (1996). The NCEP/NCAR 40-Year Reanalysis Project [Data set]. , *77*, 437–472. https://doi.org/10.1175/1520-0477(1996)077<0437:tnyrp>2.0.co;2

Kumar, A., & Hu, Z.-Z. (2014). Interannual and interdecadal variability of ocean temperature along the equatorial Pacific in conjunction with ENSO. *Climate Dynamics*, *42*(5–6), 1243–1258. https://doi.org/10.1007/s00382-013-1721-0

Lee, C. W., Tseng, Y. H., Sui, C. H., Zheng, F., & Wu, E. T. (2020). Characteristics of the prolonged El Niño events during 1960-2020. *Geophysical Research Letters*, *47*. https://doi.org/10.1029/2020GL088345

Li, X., Hu, Z. Z., Liang, P., & Zhu, J. (2019). Contrastive influence of ENSO and PNA on variability and predictability of North American winter precipitation. *Journal of Climate*, *32*(19), 6271–6284. https://doi.org/10.1175/JCLI-D-19-0033.1

Lopez, H., & Kirtman, B. P. (2014). WWBs, ENSO predictability, the spring barrier and extreme events. *Journal of Geophysical Research*, *119*. https://doi.org/10.1002/2014JD021908

Luo, J. J., Masson, S., Behera, S. K., & Yamagata, T. (2008). Extended ENSO predictions using a fully coupled ocean–atmosphere model. *Journal of Climate*, *21*(1), 84–93. https://doi.org/10.1175/2007JCLI1412.1

Masuda, S., Matthews, J. P., Ishikawa, Y., Mochizuki, T., Tanaka, Y., & Awaji, T. (2015). A new approach to El Niño prediction beyond the spring season. *Science Reports*, *5*, 16782. https://doi.org/10.1038/srep16782

Matei, D., Keenlyside, N., Latif, M., & Jungclaus, J. (2008). Subtropical forcing of tropical pacific climate and decadal ENSO Modulation. *Journal of Climate*, *21*, 4691–4709. https://doi.org/10.1175/2008jcli2075.1

McPhaden, M. J. (2003). Tropical Pacific Ocean heat content variations and ENSO persistence barriers. *Geophysical Research Letters*, *30*. https://doi.org/10.1029/2003GL016872

Mu, M., Xu, H., & Duan, W. (2007). A kind of initial errors related to "spring predictability barrier" for El Niño events in Zebiak-Cane model. *Geophysical Research Letters*, *34*. https://doi.org/10.1029/2006gl027412

Philander, S. G. (1990). *El Niño, La Niña, and the Southern Oscillation*. Academic Press, London, 293.

Rayner, N. A. (2003). Global analyses of sea surface temperature, sea ice, and night marine air temperature since the late nineteenth century [Data set]. , *108*(D14). https://doi.org/10.1029/2002JD002670

Saji, N., Goswami, B., Vinayachandran, P., & Yamagata, T. (1999). A dipole mode in the tropical Indian Ocean. *Nature*, *401*, 360–363. https://doi.org/10.1038/43854

Taylor, K. E., Stouffer, R. J., & Meehl, G. A. (2012). An overview of CMIP5 and the experiment design [Data set]. , *93*, 485–498. https://doi.org/10.1175/bams-d-11-00094.1

Terray, P. (2010). Southern Hemisphere extra-tropical forcing: A new paradigm for El Niño-Southern Oscillation. *Climate Dynamics*, *36*(11–12), 2171–2199. https://doi.org/10.1007/s00382-010-0825-z

Thirumalai, K., DiNezio, P. N., Okumura, Y., & Deser, C. (2017). Extreme temperatures in Southeast Asia caused by El Niño and worsened by global warming. *Nature Communications*, *8*, 15531. https://doi.org/10.1038/ncomms15531

Timmermann, A., Coauthors, S.-I., Kug, J.-S., Jin, F.-F., Cai, W., Capotondi, A., et al. (2018). El Niño-Southern Oscillation complexity. *Nature*, *559*, 535–545. https://doi.org/10.1038/s41586-018-0252-6

Torrence, C., & Webster, S. (1998). The annual cycle of persistence in the El Niño/Southern Oscillation. *Quarterly Journal of the Royal Meteorological Society*, *124*, 1985–2004. https://doi.org/10.1002/qj.49712455010

Trenberth, K. E. (1997). The definition of El Niño. *Bulletin of the American Meteorological Society*, *78*, 2771–2778. https://doi.org/10.1175/1520-0477(1997)078<2771:tdoeno>2.0.co;2

Troup, A. J. (1965). The 'southern oscillation. *Quarterly Journal of the Royal Meteorological Society*, *91*, 490–506. https://doi.org/10.1002/qj.49709139009

Tseng, Y. H., Hu, Z. Z., Ding, R. Q., & Chen, H. C. (2016). An ENSO prediction approach based on ocean conditions and ocean–atmosphere coupling. *Climate Dynamics*, *48*, 2025–2044. https://doi.org/10.1007/s00382-016-3188-2

Vimont, D. J., Battisti, D. S., & Hirst, A. C. (2003). The seasonal footprinting mechanism in the CSIRO general circulation models. *Journal of Climate*, *16*, 2653–2667. https://doi.org/10.1175/1520-0442(2003)016<2653:tsfmit>2.0.co;2

Vimont, D. J., Wallace, J. M., & Battisti, C. (2003). The seasonal footprinting mechanism in the Pacific: Implications for ENSO. *Journal of Climate*, *16*, 2668–2675. https://doi.org/10.1175/1520-0442(2003)016<2668:tsfmit>2.0.co;2

Walker, G., & Bliss, E. (1932). World weather V. Memoris. *Nature*, *4*, 53–84.

Wallace, J. M., & Gutzler, D. S. (1981). Teleconnections in the geopotential height field during the Northern Hemisphere winter. *Monthly Weather Review*, 784–812. https://doi.org/10.1175/1520-0493(1981)109<0784:titghf>2.0.co;2

Wang, X., Chen, M., Wang, C., Yeh, S. W., & Tan, W. (2018). Evaluation of performance of CMIP5 models in simulating the North Pacific Oscillation and El Niño Modoki. *Climate Dynamics*.

Wang, X., Guan, C., Huang, R. X., Tan, W., & Wang, L. (2018). The roles of tropical and subtropical wind stress anomalies in the El Niño Modoki onset. *Climate Dynamics*. Retrieved from https://doi.org/10.1007/s00382-018-4534-3

Wang, X., Tan, W., & Wang, C. (2018). A new index for identifying different types of El Niño Modoki events. *Climate Dynamics*, *50*(7), 2753–2765. https://doi.org/10.1007/s00382-017-3769-8

Wang, Z., Han, L., Zheng, J., Ding, R., Li, J., Hou, Z., & Chao, J. (2021). Evaluation of the Performance of CMIP5 and CMIP6 Models in Simulating the Victoria Mode–El Niño Relationship. *Journal of Climate*, *34*, 7625–7644.

Webster, P. J., & Yang, S. (1992). Monsoon and ENSO: Selectively interactive systems. *Quarterly Journal of the Royal Meteorological Society*, *18*, 877–926. https://doi.org/10.1002/qj.49711850705

Wittenberg, A. T., Rosati, A., Delworth, T. L., Vecchi, G. A., & Zeng, F. (2014). ENSO modulation: Is it decadally predictable? *Journal of Climate*, *27*, 2667–2681. https://doi.org/10.1175/jcli-d-13-00577.1

Wright, P. (1985). The Southern Oscillation: An ocean–atmosphere feedback system? *Bulletin of the American Meteorological Society*, *66*, 398–412. https://doi.org/10.1175/1520-0477(1985)066<0398:tsoaoa>2.0.co;2

Xie, S., & Philander, S. (1994). A coupled ocean-atmosphere model of relevance to the ITCZ in the eastern Pacific. *Tellus*, *46*(4), 340–350. https://doi.org/10.1034/j.1600-0870.1994.t01-1-00001.x

Yeh, S. W., Wang, X., Wang, C., & Dewitte, B. (2015). On the relationship between the North Pacific climate variability and the central Pacific El Niño. *Journal of Climate*, *28*(2), 663–677. https://doi.org/10.1175/JCLI-D-14-00137.1

Yu, J. Y. (2005). Enhancement of ENSO's persistence barrier by biennial variability in a coupled atmosphere-ocean general circulation model. *Geophysical Research Letters*, *32*. https://doi.org/10.1029/2005gl023406

Yu, J. Y., & Fang, S. W. (2018). The distinct contributions of the seasonal footprinting and charged-discharged mechanisms to ENSO complexity. *Geophysical Research Letters*, *45*(13), 6611–6618. https://doi.org/10.1029/2018GL077664

Yu, J. Y., & Kao, H. Y. (2007). Decadal changes of ENSO persistence barrier in SST and ocean heat content indices: 1958-2001. *Journal of Geophysical Research: Atmospheres*, *112*(D13). https://doi.org/10.1029/2006JD007654

Yu, J. Y., Kao, H. Y., & Lee, T. (2010). Subtropics-related interannual sea surface temperature variability in the central equatorial Pacific. *Journal of Climate*, *23*(11), 2869–2884. https://doi.org/10.1175/2010JCLI3171.1

Yu, J. Y., & Kim, S. T. (2011). Relationships between extratropical sea level pressure variations and the central Pacific and eastern Pacific types of ENSO. *Journal of Climate*, *24*, 708–720.

Yu, J. Y., Lu, M. M., & Kim, S. T. (2012). A change in the relationship between tropical central Pacific SST variability and the extratropical atmosphere around 1990. *Environmental Research Letters*, *7*(3), 034025. https://doi.org/10.1088/1748-9326/7/3/034025

Zebiak, S. E., & Cane, W. R. (1987). A model El Niño–Southern oscillation. *Monthly Weather Review*, *115*, 2262–2278. https://doi.org/10.1175/1520-0493(1987)115<2262:ameno>2.0.co;2

Zheng, F., Fang, X. H., Zhu, J., Yu, J. Y., & Li, X. C. (2016). Modulation of Bjerknes feedback on the decadal variations in ENSO predictability. *Geophysical Research Letters*, *43*(12), 560–568. https://doi.org/10.1002/2016gl071636

Zheng, F., Wang, H., & Zhu, J. (2009). ENSO ensemble prediction: Initial error perturbations vs. model error perturbations. *Chinese Science Bulletin*, *54*, 2516–2523. https://doi.org/10.1007/s11434-009-0179-2

Zhu, J., Kumar, A., Huang, B., Balmaseda, M. A., Hu, Z. Z., Marx, L., & Kinter, J. L. (2016). The role of off-equatorial surface temperature anomalies in the 2014 El Niño prediction. *Scientific Reports*, *6*. https://doi.org/10.1038/srep19677